

## Science Forum (Journal of Pure and Applied Sciences)



Journal Homepage: <a href="https://atbuscienceforum.com.ng/index.php/jpas">https://atbuscienceforum.com.ng/index.php/jpas</a>

Geochemistry, Depositional Environment, and Economic Potential of the Toto-Muro Banded Iron Formation, North-Central Nigeria

Daspan, R.I., Diyelmak, V.B., Bunyaminu, I. Department of Geology, University of Jos

#### **Abstract**

The Toto-Muro Banded Iron Formation (BIF) in north-central Nigeria is a Precambrian iron deposit whose geochemical characteristics provide insights into its genesis, depositional environment, and economic significance. Major and trace element geochemistry, including Fe<sub>2</sub>O<sub>3</sub>, SiO<sub>2</sub>, and Al<sub>2</sub>O<sub>3</sub> concentrations, indicate a dominant hydrothermal origin with minimal detrital input, as confirmed by MnO/TiO2 vs. Fe<sub>2</sub>O<sub>3</sub>/TiO<sub>2</sub> and Fe-Mn-Al ternary plots. Rare earth element (REE) patterns exhibit light REE (LREE) enrichment, weak to moderate Eu anomalies, and Y/Ho ratios ranging from 3.5 to 51, suggesting a mixed hydrothermal-seawater depositional environment. The presence of negative Eu anomalies in some samples reflects increasing atmospheric oxygenation during the Paleoproterozoic (Planavsky et al., 2012). Tectonically, the deposit is consistent with passive margin to back-arc basin settings, similar to other West African BIFs. Comparisons with BIFs in Cameroon highlight variations in detrital input and tectonic evolution. Economically, the high Fe2O3 content and low concentrations of deleterious elements (Ti, Al, and P) indicate potential for direct shipping ore (DSO) suitability, enhancing its viability for iron and steel industries. This study provides critical insights into the geodynamic evolution of the region and underscores the economic importance of the Toto-Muro BIF in Nigeria's mineral resource sector.

Keywords
Banded Iron Formation,
Geochemistry,
Hydrothermal Alteration,
Rare Earth Elements,
Toto-Muro Deposit

#### 1. Introduction

Banded Iron Formations (BIFs) were deposited predominantly during the Precambrian era, with the majority forming between ~3.8 and 1.0 billion years ago (Ga). These iron-rich sedimentary deposits typically exhibit low to moderate iron content (15-35% Fe) but occur in vast tonnages, often extending laterally for hundreds to thousands of kilometers and reaching significant thicknesses. BIFs are widely accepted as chemical precipitates of Fe<sup>2+</sup> and Fe<sup>3+</sup> oxides, hydroxides, Fe-rich silicates, and silica in marine environments, followed by diagenesis and metamorphism. According to Gross (1980), BIFs are classified into two main types: (1) the Algoma-type, with submarine volcanoassociated sedimentary settings, typical of the Archean, and (2) the Superior-type, deposited in shallow marine environments with some continental input, mainly during the Paleoproterozoic.

The Toto-Muro Banded Iron Formation (BIF) is one of Nigeria's significant iron deposits, located within the Toto-Muro Proterozoic metasedimentary schist belt. longitudes 7°14′00″E and 7°17′00″E latitudes 8°21'00"N and 8°19'50"N, as mapped on Katakwa NE sheet 228 (Fig. 1). The associated formation. along with metasedimentary rocks, forms prominent NE-SW trending rugged hills stretching approximately 13 km. Discovered by the Geological Survey of Nigeria in 1981, the deposit has been the subject of several geological and geochemical studies (Muotoh et al., 1979; Nnagha et al., 1984; Umeji, 1984; Muotoh et al., 1988; Anike et al., 1990, 1993; Oladepo, 1990). Adekoya et al. (2012) conducted a detailed geochemical analysis, reporting trace element compositions for the first time. This study expands on previous research by providing a more comprehensive geochemical characterization, including major, trace, and rare earth element (REE) analyses, to classify the deposit and propose its genetic model.

## 2. Geologic Setting

2.1 Regional Geologic Setting and Geology of the Study Area.

The Toto-Muro Banded Iron Formation forms part of the Toto Schist belt which forms the supracrustal rocks of Nigeria which are found west of longitude 8° and are Paleoproterozoic and Neoproterozoic in age. They form part of the Nigerian basement which itself constitutes the southern part of Neoproterozoic Pan-African mobile belt situated east of the West African craton. They have been affected by multiple deformation and metamorphism (8) and are made of pelitic and and semi-pelitic schists and phyllites interlayered with minor to substantial metaquartzites?. They consist essentially of pelitic and semi-pelitic schists and phyllites interlayered with minor to substantial quartzites, metaconglomerate, iron-formation, marble and amphibolite of tholeiitic affinity. The main deformation phase (D2) produced major folds such as the Muro antiform in the study area. Both the basement and its supracrustal cover (the Schist Belts) have been intruded by a suite of Pan-African granites (Older Granites) with minor contact metamorphic and local migmatization effects in the host rocks during the Pan African orogeny (ca 600 ± 150 Ma).

## 2.2. Geology of the Study Area

The Toto-Muro area is made up of four major lithological units which are interbedded (Figure 2). They are mainly marble, banded iron formation, quartzites and metasediments which are pelitic to semi-pelitic in composition. All the lithologies are variously folded with the marble occupying both the inner core and flanks of the fold. These are followed in a successive pattern by bands of pelitic and semi-pelitic metasediments, quartzites and banded iron formation. Towards the western end of the the Muro hills the metasediments are overlain unconformably by the Cretaceous Nupe Sandstone.(Adekoya, 2013). The BIF occur in bands between 35-100m thick/thick and occur between the outer zone marble and quartzites. They form arcuate Muro Antiform elongate ridges and irregular hills which extend for 20 km. Two-fold types are recognised two generations of minor folds which are tight, isoclinals, overturned folds having attenuated limbs with thickened or sharp crests and open folds with nearly horizontal axes. According to both oxide and carbonate facies occur but the oxide facies predominates. The oxide facies iron formation dark grey, fine-grained, crystalline rock which displays banding on both centimetre and millimetre scales (i.e meso- and microbanding). The banding consists of alternating light-coloured quartz-rich and darker-coloured iron oxide-rich layers. The mesobands range in width from about 1cm to 2cm and the microbands from ,0.5-2cm (Plate 1b)

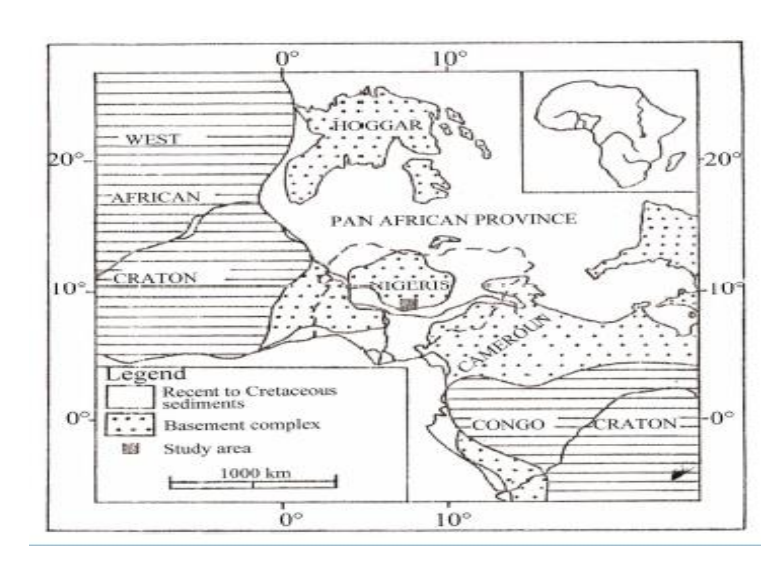


Figure 1: Location map of the Toto Muro Banded Iron Formation (Adapted from Adekoya, et.al, 2012)

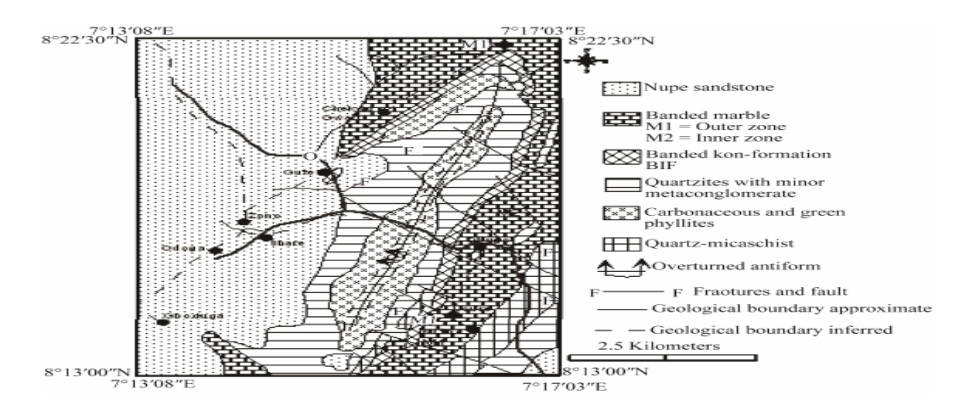


Figure 2: Geological map of the Toto-Muro area showing the occurrence of the Banded Iron Formation. (Adapted from Adekoya, et.al, 2012



Plate 1a and b: Scattered boulders of Banded Iron Formation and Meso and microbanding in Toto Muro Banded Iron Formation



Plate 2. A folded block of Toto Muro Banded Iron Formation

#### 3. Materials and Methods.

Ten (10) samples were selected for major, trace and rare earth element analyses. All the samples were grounded to powder in an agate mortar in the Geochemistry Laboratory of the Geology Department, University of Jos. 0.2 g of each sample was weighed into a graphite crucible and mixed with 1.5g of LiBO<sub>2</sub>/LiB<sub>4</sub>O<sub>7</sub>. The sample charge was heated in a muffle furnace for 30 min at 980° C. The cooled bead is dissolved in 100 mL of 5 % HNO3 (ACS grade nitric acid in de-mineralized water). An aliquot of the solution was poured into a propylene tube. Calibration standards verification standards are included in the sample sequence. Sample solutions are aspirated into an ICP mass spectrometer Elmer Elan 9000) (Perkinfor determination of major, minor and rare earth elements at the Acme Laboratories in Vancouver. Canada. A 0.25q split is heated in HNO<sub>3</sub>-HClO<sub>4</sub>-HF to fuming and taken to dryness. The residue is dissolved in HCl. Solutions are analysed by your choice of the Coupled Plasma-Mass Inductively Spectrometer. The following major elements were analyzed: TiO2, Al2O3, Fe2O3, CaO, MgO,  $Na_2O$ ,  $K_2O$ ,  $P_2O_5$  and S. The trace elements analyzed are Mo, Cu, Pb, Zn, Aq, Ni, Co, Cu, As, Au, Sr, Cd, Sb, Bi, V, Cr, Ba, W, Zr, Sn, Be, Sc, Y, Hf, Li, Rb, Ta, Nb, Cs, Th and U while the rare earth elements analysed are La, Ce, Pr, Nd, Sm, Eu, Gd, Tb, Dy, Ho, Er, Tm, Yb and Lu

## 4. Results and Discussion

### 4.1 Major Elements

The major element compositions of the Toto-Muro Banded Iron Formation (BIF) are presented in Table 1. The  $SiO_2$  content ranges

from 54.99 to 84.79 wt.% (average 63.77 wt.%), while Al<sub>2</sub>O<sub>3</sub> concentrations are low, varying between 0.04% and 0.30% (average 0.13 wt.%). Fe<sub>2</sub>O<sub>3</sub> content ranges from 12.25% to 42.38% (average 34.60 wt.%), indicating significant iron enrichment in some samples. Other oxides include CaO (0.027-1.945 wt.%, average 0.43 wt.%), MgO (0.03%-1.63 wt.%, average 1.20 wt.%), and MnO (0.01%-0.79 wt.%, average 0.09 wt.%). The concentrations of K2O, TiO2, and P2O5 are consistently low, with average values of 0.02 wt.%, 0.01 wt.%, and 0.02 wt.%, respectively. The results indicate that Fe<sub>2</sub>O<sub>3</sub> concentration varies from low to high (12.25-42.38 wt.%), with the majority of samples averaging above 30 wt.%. The concentrations of Al<sub>2</sub>O<sub>3</sub>, MnO, K<sub>2</sub>O, TiO<sub>2</sub>, P2O5, and S are all below 0.5%, while the average compositions of CaO and Na2O are 0.57% and 0.42%, respectively. The calculated elemental ratios further characterize the geochemistry of the formation: Si/Al (203.56-2119.75), Fe/Ti (594.67-21190), Al/Ti (2.83-45.00), Fe/Al (128.00-647), Fe/Si (0.14-0.79), and Ti/Al (0.02-0.35). A negative correlation exists between SiO2 and Al2O3 (Figure 3a), while Fe<sub>2</sub>O<sub>3</sub> exhibits a positive correlation with TiO<sub>2</sub> (Figure 3b).

In the Zr/Ti vs. Ni protolith discrimination diagram of Winchester et al. (1980), the analyzed samples plot within the sedimentary field (Figure 5a), indicating a sedimentary origin for the Toto-Muro BIF. This suggests that the formation is composed of metasediments. Additionally, in the  $CaO-Na_2O+K_2O-Al_2O_3$  ternary geochemical affinity diagram (Radam et al., 198), all samples fall within the peraluminous domain (Figure 5b), a characteristic feature of sedimentary-derived

rocks (Shand, 1943). Binary plots of Fe<sub>2</sub>O<sub>3</sub> (T) against other major oxides (Figure 5) reveal key geochemical trends. CaO and SiO2 concentrations decrease with increasing Fe<sub>2</sub>O<sub>3</sub>, while all other oxides show an increasing trend with Fe<sub>2</sub>O<sub>3</sub> enrichment. The binary plots show a negative correlation between  $Fe_2O_3(T)$ and SiO2, suggesting separate precipitation processes. Weak correlations of Fe<sub>2</sub>O<sub>3</sub>(T) with Al2O3 and TiO2 indicate minimal detrital input, confirming a predominantly hydrothermal origin. The positive Fe<sub>2</sub>O<sub>3</sub>(T)-MnO correlation supports hydrothermal influence, while low P2O5 suggests limited biological activity during deposition. The geochemical composition of the Toto-Muro BIF was compared with various BIF occurrences worldwide (Table 2). The results indicate that the studied BIF shares similarities with the Lake Superior-type BIF and Orissa-type BIF, though with a lower Fe<sub>2</sub>O<sub>3</sub> concentration than both. Compared to global BIF types, the study area BIF exhibits lower Al<sub>2</sub>O<sub>3</sub> and Fe<sub>2</sub>O<sub>3</sub> concentrations. MgO concentrations in the Toto-Muro BIF are similar to those of the Lake Superior-type and Tamil Nadu, India-type BIFs but are higher than those of the Orissa-type BIF and lower of Algoma, than those Archean. Proterozoic BIFs. MnO concentrations in the study area BIF are higher than in the Orissatype BIF but lower than in other BIF occurrences.These geochemical characteristics suggest that the Toto-Muro BIF is of sedimentary origin, with possible hydrothermal influences during its formation. The observed compositional variations relative to other BIFs indicate differences in depositional conditions, clastic input, and iron precipitation mechanism

Table 1: Major Element (wt. %) Composition of the Toto-Muro Banded Iron Formation

Oxide/Ratio	TMBIF	TMBIF	TMBI	TMBI	TMBIF	TMBI	TMBI	TMBI	TMBI	TMBIF
Oxide/Rullo	1	2	F3	F4	5	F6	F7	F8	F9	10
SiO <sub>2</sub>	55.39	56.75	61.07	84.79	58.75	69.22	70.86	64.27	64.51	54.33
Fe <sub>2</sub> O <sub>3</sub>	42.38	40.39	38.40	12.25	38.83	30.05	29.51	35.62	35.68	42.94
Al2O3	0.09	0.11	0.30	0.04	0.06	0.10	0.12	0.08	0.17	0.19
CaO	0.03	0.25	0.07	1.95	0.03	0.14	0.10	0.02	0.027	0.85
MgO	1.39	1.63	0.03	0.90	2.33	0.02	0.02	0.02	0.53	1.59
MnO	0.003	0.002	0.003	0.01	0.04	0.45	0.37	0.004	0.02	0.05
Na <sub>2</sub> O	0.65	0.79	0.03	0.01	0.002	0.002	0.002	0.002	0.003	0.003
K <sub>2</sub> O	0.02	0.02	0.02	0.02	0.01	0.01	0.01	0.01	0.02	0.02
TiO <sub>2</sub>	0.002	0.003	0.01	0.003	0.002	0.01	0.01	0.01	0.06	0.02
P2O5	0.04	0.05	0.06	0.02	0.01	0.03	0.03	0.01	0.003	0.002
LOI	0.10	0.72	0.83	0.14	0.13	0.10	1.06	0.73	1.07	0.51
Total	99.90	99.28	99.17	99.86	99.87	99.90	99.94	99.27	99.93	99.49

Oxide/Ratio		TMBIF 2		TMBI F4	TMBIF 5			TMBI F8	TMBI F9	TMBIF 10
Si/Al	615.44	515.91	203.5 7	2119.7 5	979.17	692.2 0	l_	803.3 8	379.4 7	285.95
Fe/Ti	21190. 00	13463. 33	3840. 00	4083. 33	19415. 00	3005. 00	2951.0 0	3562. 00	594.6 7	2147.0 0
Al/Ti	45.00	36.67	30.00	13.33	30.00	10.00	12.00	8.00	2.83	9.50
Fe/Al	470.89	367.18	128.00	306.2 5	647.17	300.5 0	l_	445.2 5	209.8 8	226.00
Fe/Si	0.77	0.71	0.63	0.14	0.66	0.43	0.42	0.55	0.55	0.79
Ti/Al	0.02	0.03	0.03	0.08	0.03	0.10	0.08	0.13	0.35	0.11
SiO2/Fe2O3	1.31	1.41	1.59	6.92	1.51	2.30	2.40	1.80	1.81	1.27
(MgO+CaO+MnO)/ Fe2O3	0.03	0.05	0.00	0.23	0.06	0.02	0.02	0.00	0.02	0.06

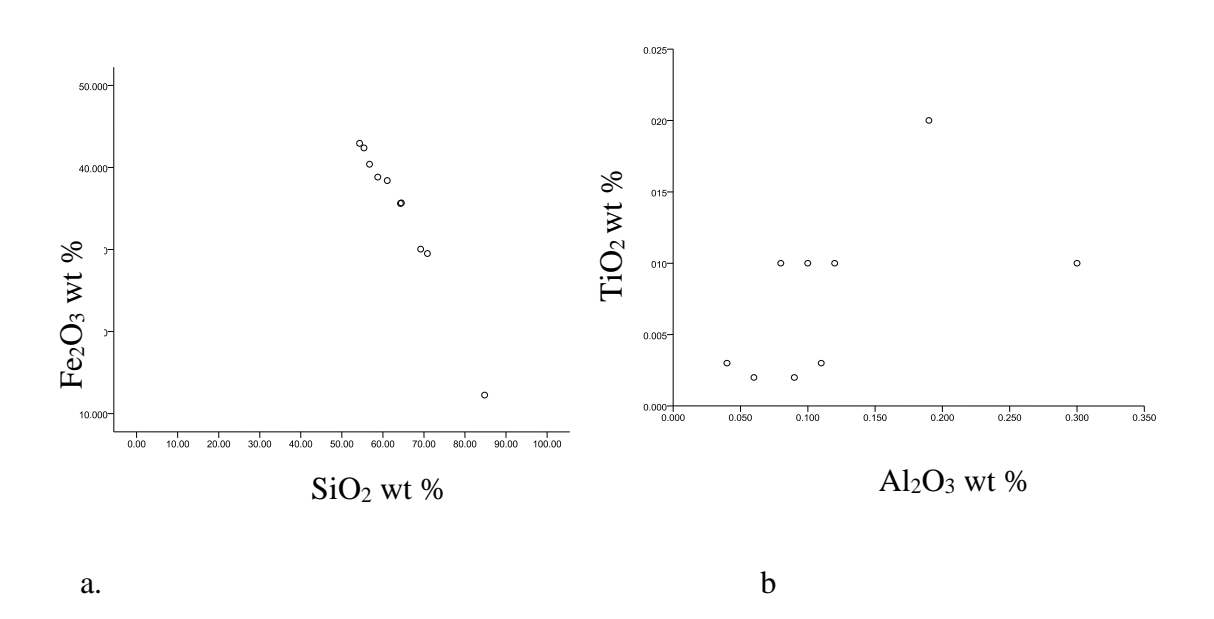


Figure 3a  $SiO_2$  wt.% vs  $Al_2O_3$  wt.% plot for the Toto-Muro Banded Iron Formation (BIF) showing conspicuous decrease in  $Fe_2O_3$  as  $SiO_2$  increases. Figure 3b:  $Al_2O_3$  wt. % vs  $TiO_2$  wt. % plot for the Toto-Muro Banded Iron Formation (BIF) showing an increase in  $Al_2O_3$  as  $TiO_2$  increases.

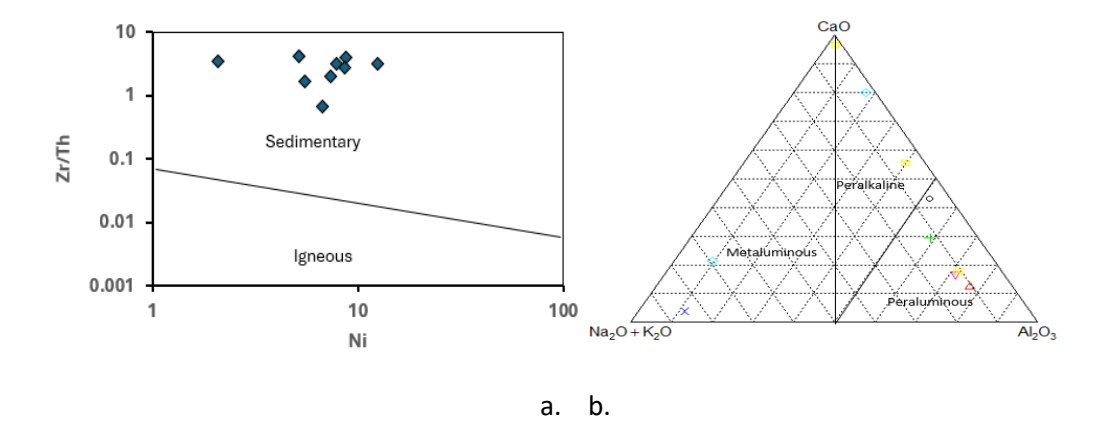
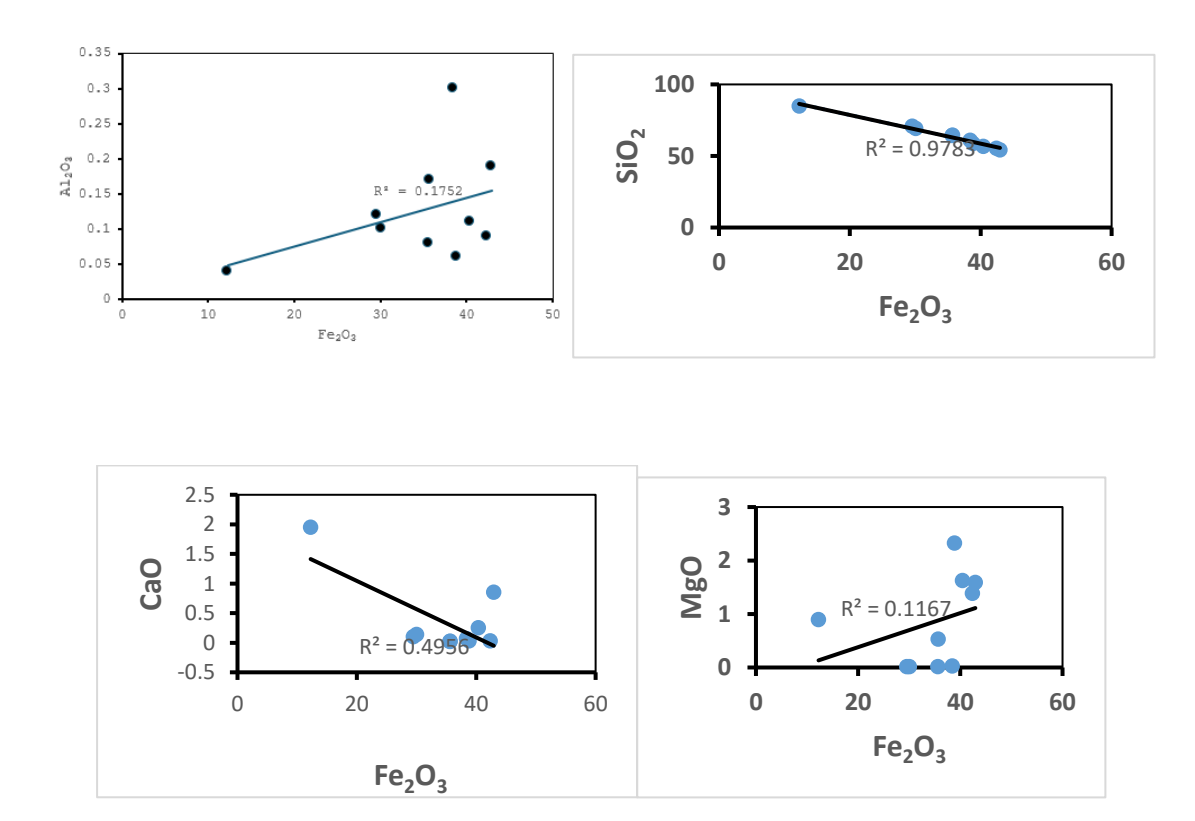


Figure 4a: Chemical Discrimination of the Toto Muro Banded Iron Formation (a).Plot of the Toto Muro Banded Iron Formation (BIF) in the Zr/Ti vs Ni (ppm) discrimination diagram after Winchester, J. A., Park, K. G., Holland, J. G. (1980). (b) Position of the Toto Muro Banded Iron Formation within the ternary diagram CaO-Na2O + K2O-Al<sub>2</sub>O<sub>3</sub> after Lasserre, M., Chatonier, D. (1958).



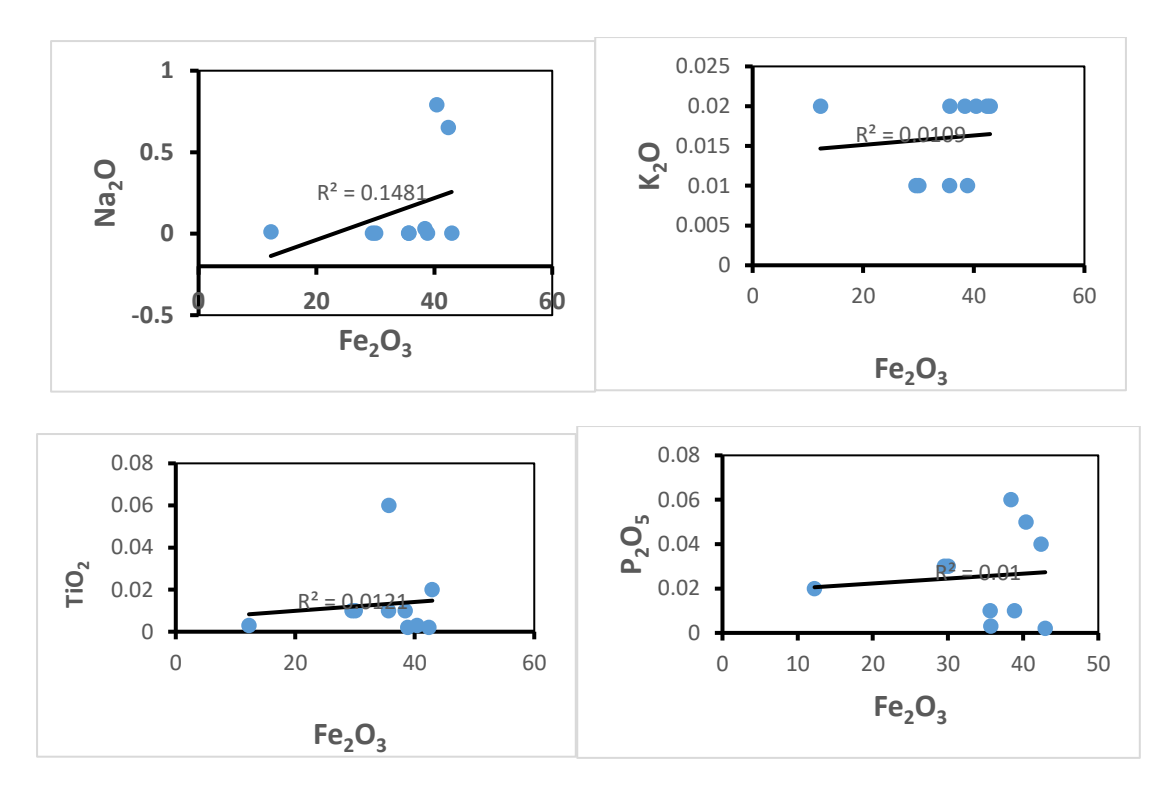


Figure 5. Binary graphs for selected major elements against Fe2O3(T).

Table 2: Comparison of Major Element (wt. %) Concentration of the Toto-Muro BIF with

Other BIF Types Worldwide

Oxide/Constituent	1	2	3	4	5	6	7	8	9	10	11	12	13
SiO₂	63.77	57.66	_	50.50	47.20	47.30	46.90	47.02	44.62	67.02	49.07	48.20	_
Fe <sub>2</sub> O <sub>3</sub>	34.60	38.29	_	41.33	44.51	45.79	43.76	53.33	53.21	53.21	18.98	29.09	
Al <sub>2</sub> O <sub>3</sub>	0.13	0.28	_	3.00	1.39	1.25	1.15	0.70	0.35	1.10	0.70	0.42	_
MgO	0.43	0.01	_	1.53	1.24	3.66	4.41	0.13	1.21	1.21	3.46	2.39	_
CaO	1.20	0.02	_	1.51	1.58	2.84	4.43	0.17	0.70	0.22	2.68	1.80	
MnO	0.09	0.06	_	0.22	0.73	0.59	0.59	0.06	0.23	0.01	0.55	0.08	_
Na2O	0.25	0.01	_	0.31	0.12	0.22	0.29	0.10	0.23	0.20	0.11	0.49	
K <sub>2</sub> O	0.02	0.02	_	0.58	0.14	0.09	0.48	0.13	0.17	0.42	_	0.71	
P2O5	0.01	0.05	_	0.21	0.06	0.22	0.14	0.07	0.28	0.11	0.16	0.22	

1. Average of this study area BIF. 2. Average of Toto Muro oxide facies (Adekoya, 2012), 3. Average of Toto Muro silicate facies (Adekoya, 2012) 4. Average Algoma-type oxide facies 5. Average Lake Superior-type. 6. Average Archean BIF 7. Average Proterozoic BIF. 8. Average of Orissa BIF. 9. Average of Tamil Nadu, India BIF. 10. Average of Sukumaland, Tanzania 11. verage BIF Yilgarn Black Australia 11. Brockman Iron Formation 12. Biwabik Iron Formation

## 4.2 Trace Element Geochemistry

The trace element composition of the Toto-Muro Banded Iron Formation (BIF) is presented in Table 3, with comparisons to other BIFs worldwide in Table 4. The results indicate notable variations in trace element concentrations, which are discussed below.

## 4.2.1 Large Ion Lithophile Elements (LILEs) (Ba, Rb, Sr, Pb)

Barium (Ba): The concentration of Ba in the Toto-Muro BIF ranges from 17 to 226 ppm, with an average of 74.3 ppm. This value is higher than the 9-93 ppm range reported by Adekoya (2015) for the oxide facies of the Muro BIF but lower than those recorded in other BIFs globally (Table 4). Rubidium (Rb): The Toto-Muro BIF is significantly depleted in Rb, with values ranging from 0.1 to 0.8 ppm (average 0.3 ppm). Adekoya (2015) reported Rb concentrations below the detection limit (<5 ppm) in the Muro BIF (Table 5). Strontium (Sr): Sr content in the Muro BIF is relatively low, ranging from 4 to 13 ppm (average 7.4 ppm). This is lower than the averages for the Lake Superior-type BIF, the Algoma-type silicate facies BIF, and the Orissa oxide facies but higher than the Maru BIF (Table 4).Lead (Pb): The Pb concentration varies between 5.96 and 21.59 ppm (average 13.54 ppm). Adekoya (2015) similarly noted Pb depletion in the Muro BIF compared to other BIFs worldwide (Table 4).

# 4.2.2 Transition Elements (V, Co, Ni, Zn, Cu, Cr)

Vanadium (V): The Toto-Muro BIF contains 2-9 ppm of V (average 6.4 ppm), which is lower than the 12 ppm reported for the oxide facies and significantly lower than the 100 ppm

recorded in the carbonate facies of the Muro BIF (Adekoya, 2015). This trend is also observed in the Lake Superior-type BIF (Table 4).Cobalt (Co): Co concentrations in the Muro BIF range from 0.7 to 2.2 ppm (average 1.27 ppm). These values are markedly lower than the 128-194 ppm reported by Adekoya (2015). Compared to other BIFs (Table 4), the Lake Superior-type, Algoma-type, Orissa BIF, and Minas Gerais itabirite all contain higher Co concentrations than the Toto-Muro BIF. Nickel (Ni): Ni concentrations range from 0.3 to 12.5 ppm (average 6.51 ppm). Adekoya (2015) reported similarly low Ni values (<10-26 ppm) in the Muro BIF, particularly in the oxide facies (<10 ppm).

The Ni content of the Toto-Muro BIF is lower than that of the Lake Superior-type and Algoma-type BIFs but comparable to the Orissa BIF and the Minas Gerais itabirite (Table 4).Zinc (Zn): Zn concentrations range from 3.2 to 10.4 ppm (average 6.77 ppm). Adekoya (2015) also noted Zn depletion in the Muro BIF relative to other global BIFs (Table 4).Copper (Cu): Cu concentrations range from 1.45 to 25.34 ppm (average 13.54 ppm). This is lower than the 40 ppm mean reported by Adekoya (2012) for the Toto-Muro oxide facies but comparable to the Lake Superior-type (oxide facies), Orissa BIF, and Minas Gerais itabirite (Table 4).Chromium (Cr):

The Cr content in the Toto-Muro BIF is relatively high, ranging from 127 to 434 ppm (average 133.40 ppm). Adekoya (2015) reported lower Cr concentrations in the Muro oxide facies (10-19 ppm) and carbonate facies (12-24 ppm). Compared to other BIFs (Table 4), the Cr concentration in the Toto-Muro BIF

is higher than that in the Minas Gerais itabirite and Orissa BIF. Low Cr concentrations have also been reported in Swedish iron ores and sedimentary BIFs (Ganno et al., 2018; Eka Nzume et al., 2018).

# 4.2.3 High Field Strength Elements (HFSEs) (Y, Zr, Th, U, Nb)

Yttrium (Y): Y concentrations are very low, ranging from 0.7 to 10.2 ppm (average 2.66 ppm). These values are lower than those reported by Adekoya (2015), who found that the Toto-Muro BIF contained minimal or no Y.Zirconium (Zr): Zr content is also low, ranging from 0.5 to 2.6 ppm (average 1.51 ppm). This is lower than the Zr concentrations reported for the Toto-Muro BIF by Adekoya (2015) and other BIFs (Table 5). The Zr content in the Toto-Muro BIF is also lower than that of the Lake Superior-type and Algoma-type BIFs. Rai and Paul (1990, cited in Adekoya, 2015) suggested that since Zr distribution is more related to sediment provenance than sorting, the low Zr levels in the Muro BIF indicate derivation from a low-Zr source material, supporting a sedimentary rather than igneous origin. Thorium (Th): Th concentrations are low, ranging from 0.3 to 1.8 ppm (average 0.66 ppm).

Adekoya (2015) reported values between 5 and 12 ppm, with most samples falling below the detection limit (5 ppm, Table 5). Th data for other BIFs is unavailable. Uranium (U): U concentrations are very low, ranging from 0.1 to 0.7 ppm (average 0.27 ppm). Similar low values were reported by Adekoya (2015) for both the oxide and carbonate facies, as well as for the Lake Superior and Maru BIFs (Table 4).

Data on U content in other BIFs is lacking, preventing further comparisons. Niobium (Nb): Nb concentrations range from 0.62 to 3.48 ppm (average 1.47 ppm), which is lower than values reported for the Maru BIF (Adekoya, 2012). Adekoya (2015) also reported low Nb concentrations for both the oxide and carbonate facies of the Toto-Muro BIF. Due to limited Nb data for other BIFs, comparisons are difficult.

## 4.2.4 General Trends and Normalization Patterns

Overall, the trace element composition of the Muro BIF closely resembles that of the Lake Superior-type oxide facies, except for its lower Ba and Cr contents and higher Co concentrations. The Muro BIF also exhibits significantly lower concentrations of Ba, Cr, Cu, Ti, V, and Zr compared to the Algoma-type BIF (Table 4).

- NMORB-normalized Spider Diagrams (Figure 5): The Toto-Muro BIF is enriched in Cs, Ba, Th, U, La, and Pb but depleted in Rb, K, P, Nd, Zr, Sm, Eu, Th, Y, Yb, and Lu.
- Primitive Mantle-normalized Spider
  Diagrams (Figure 6): The Toto-Muro
  BIF is enriched in Cs, Ba, Th, U, Nb,
  Ta, La, and Pb but depleted in Sr, P,
  Zr, and Ti.
- Average Crust-normalized Trace
   Element Spider Diagram (Figure 7):
   The Toto-Muro BIF shows an overall
   depletion of all elements compared to
   the average crust, with distinct
   depletion in K and TI (Weaver &
   Turner, 1984).

Table 3: Trace Element Concentrations of the Toto Muro Banded Iron Formation (Bif)

Element	1	2	3	4	5	6	7	8	9	10	Min	Max	Average
Мо	4.48	4.28	3.89	7.24	3.72	6.44	4.7	4.1	13.2	3.71	3.71	13.2	5.58
Cu	1.45	2.09	6.92	3.75	1.54	25.36	24.09	1.71	4.07	2.07	1.45	25.36	7.30
Pb	5.96	8.41	16.07	21.59	11.49	19.15	11.73	9.57	20.65	10.79	5.96	21.59	13.54
Zn	7.5	6.0	10.4	5.0	8.3	6.0	4.8	3.2	6.1	10.4	3.2	10.4	6.77
Ag	26.0	31.0	35.0	22.0	27.0	38.0	32.0	43.0	37.0	29.0	22.0	43.0	32.00
Ni	8.8	7.4	7.9	6.7	5.5	8.7	2.1	0.3	12.5	5.2	0.3	12.5	6.51
Со	1.0	0.9	1.8	0.7	0.7	2.2	1.8	2.1	8.0	0.7	0.7	2.2	1.27
As	1.3	0.6	2.3	0.7	0.4	3.9	4.4	0.5	1.1	0.5	0.4	4.4	1.57
Au	<0.1	<0.1	<0.1	<0.1	<1.0	<1.0	<1.0	<1.0	<0.1	0.1	<0.1	0.1	0.10
Sr	5.0	6.0	4.0	7.0	4.0	13.0	12.0	5.0	13.0	5.0	4.0	13.0	7.40
Cd	0.03	0.02	<0.02	<0.02	0.03	0.04	<0.02	<0.02	<0.02	<0.02	<0.02	0.04	0.03
Sb	0.39	0.65	1.1	1.04	2.75	1.87	1.23	1.15	1.71	2.69	0.39	2.75	1.46
Bi	4.28	8.52	2.3	19.66	0.97	3.07	3.0	5.64	0.16	0.74	0.16	19.66	4.83
V	2.0	<1.0	8.0	<1.0	<1.0	6.0	9.0	7.0	<1.0	<1.0	<1.0	9.0	6.40
Cr	164.0	163.0	134.0	241.0	127.0	213.0	151.0	134.0	424.0	134.0	127.0	424.0	188.50
Ва	21.0	17.0	28.0	34.0	109.0	33.0	97.0	64.0	226.0	114.0	17.0	226.0	74.30
Zr	1.6	1.2	2.6	1.2	0.5	1.7	1.4	1.3	1.9	1.7	0.5	2.6	1.51
У	0.6	8.0	8.3	0.7	2.5	1.6	1.5	0.7	10.2	1.9	0.7	10.2	3.07
Th	0.4	0.6	8.0	1.8	0.3	0.6	0.4	0.7	0.6	0.4	0.3	1.8	0.66
U	<0.1	0.1	0.7	0.1	<0.1	0.3	0.3	0.2	0.2	<0.1	<0.1	0.7	0.27
Th/U	4.00	6.00	1.14	18.00	3.00	2.00	1.33	3.50	3.00	4.00	1.14	18.00	2.44

Table 4: Averages of Chemical Analyses of Trace Elements of Banded Iron-Formations from Other Parts of the World

Element	1 (This Study)	2	3	4	5	6	7	8	9	10	11
Ва	74.30	41	924	180	170	170	70	293	70	ND	ND
Со	1.27	166	142	27	27	38	36	100	35	ND	ND
Cr	188.50	10	20	122	102	78	38	23	30	ND	ND
Cu	7.30	40	304	100	37	96	99	<10	10	1.6	ND
Mn	292	465	17,300	4,600	3,400	1,400	7,300	37,408	120	200	ND
Nb	1.47	5	7	ND	ND	ND	ND	5	ND	ND	ND

Element	1 (This Study)	2	3	4	5	6	7	8	9	10	11
Ni	6.51	<10	22	32	46	83	151	<10	15	9.7	ND
Pb	13.54	8	5	ND	ND	ND	23	10	ND	ND	ND
Rb	0.30	<b>&lt;</b> 5	<b>&lt;</b> 5	ND	ND	ND	ND	20	ND	ND	ND
Sr	7.40	18	36	42	30	83	51	15	6.0	ND	ND
Th	0.66	5	5	ND	1,900	ND	ND	6	ND	ND	ND
Ti	300	120	60	160	ND	860	1,910	959	80	ND	ND
U	0.27	9	8	ND	124	ND	ND	5	ND	ND	ND
V	6.40	12	100	30	43	97	54	44	30	16	ND
У	3.07	<b>&lt;</b> 5	8	41	ND	54	84	22	ND	ND	ND
Zn	6.77	<20	<10	2	165	33	34	26	ND	15	ND
Zr	1.51	39	42	56	165	84	267	60	10	ND	ND

#### ND = Not Determined

#### Data Sources:

- 1. Toto Muro BIF This study
- 2. Toto Muro Oxide Facies Adekoya et al., 2012
- 3. Toto Muro Carbonate Facies North America (Gross & McLeod; Suresh & Basavanna, 2014; Selmi et al., 2009)
- 4. Lake Superior Oxide Facies North America (Gross & McLeod; Suresh & Basavanna, 2014; Selmi et al., 2009)
- 5. Lake Superior Silicate Facies (Gross & McLeod; Suresh & Basavanna, 2014; Selmi et al., 2009)
- 6. Algoma Type Oxide Facies North America (Gross & McLeod, 1980)
- 7. Algoma Type Carbonate Facies North America (Gross & McLeod, 1980)
- 8. Maru BIF (Adekoya, 1988)
- 9. Orissa Oxide Facies Iron Formation, India (Majumber et al., 1982)
- 10. Itakpe BIF (Mücke & Neumann, 1986)
- 11. Kakun Iron Ore (Abhulmen, 1986)
- 12. Gangfelum Iron Formation (Bolarinwa, 2018)
- 13. Itabarite from Minas Gerais, Brazil (Majumder et al., 1982)

Table 4: Averages of Chemical Analyses of Trace Elements of Banded Iron-Formations from other Parts of the World.

Element	1	2	3	4	5	6	7	8	9	10	11	12	13	Average
Ва	74.30	41	924	180	170	170	70	293	70	ND	ND	ND	ND	221.37
Со	1.27	166	142	27	27	38	36	100	35	ND	ND	ND	ND	63.59
Cr	188.50	10	20	122	102	78	38	23	30	ND	ND	ND	ND	67.94
Cu	7.30	40	304	100	37	96	99	<10	10	1.6	ND	ND	ND	77.21
Mn	292	465	17300	4600	3400	1400	7300	37408	120	200	ND	ND	ND	7248.50
Nb	1.47	5	7	ND	ND	ND	ND	5	ND	ND	ND	ND	ND	4.62
Ni	6.51	<10	22	32	46	83	151	<10	15	9.7	ND	ND	ND	45.65
Pb	13.54	8	5	ND	ND	ND	23	10	ND	ND	ND	ND	ND	11.91
Rb	0.30	<b>&lt;</b> 5	<b>&lt;</b> 5	ND	ND	ND	ND	20	ND	ND	ND	ND	ND	10.15
Sr	7.40	18	36	42	30	83	ND	51	15	6.0	ND	ND	ND	32.04
Th	0.66	5	5	ND	1900	ND	ND	6	ND	ND	ND	ND	ND	383.33
Ti	300	120	60	160	ND	860	1910	959	80	ND	ND	ND	ND	556.13
U	0.27	9	8	ND	124	ND	ND	5	ND	ND	ND	ND	ND	29.25
V	6.40	12	100	30	43	97	54	44	30	16	ND	ND	ND	43.24
У	3.07	<b>&lt;</b> 5	8	41	ND	54	84	22	ND	ND	ND	ND	ND	35.35
Zn	6.77	<20	<10	2	165	33	34	26	ND	15	ND	ND	ND	40.25
Zr	1.51	39	42	56	165	84	267	60	10	ND	ND	ND	ND	80.50

## ND=Not Determined.

- 1. Toto Muro BIF this study
- 2. Toto Muro Oxide facies Adekoya et al., 2012
- 3. Toto Muro Carbonate facies North America (Gross and Mcleod, Suresh and Basavanna, 2014, Selmi et al., 2009)
- 4. Lake Superior Oxide facies North America (Gross and Mcleod, Suresh and Basavanna, 2014, Selmi et al., 2009)
- 5. Lake Superior Silicate facies (Gross and Mcleod, Suresh and Basavanna, 2014, Selmi et al., 2009)
- 6. Algoma type oxide facies North America (Gross and Mcleod, 1980)
- 7. Algoma type Carbonate facies North America (Gross and Mcleod, 1980)
- 8. Maru BIF (Adekoya, 1988)
- 9. Orissa oxide facies iron formation, India (Majumber et al., 1982)
- 10. Itakpe BIF Mucke, A. and Neumann, U. (1986)
- 11. Kakun iron ore Abhulmen (1986)
- 12. Gangfelum iron formation Bolarinwa (2018)
- 13. Itabarite from Minas Gerais, Brazil Majumder et al. (1982)

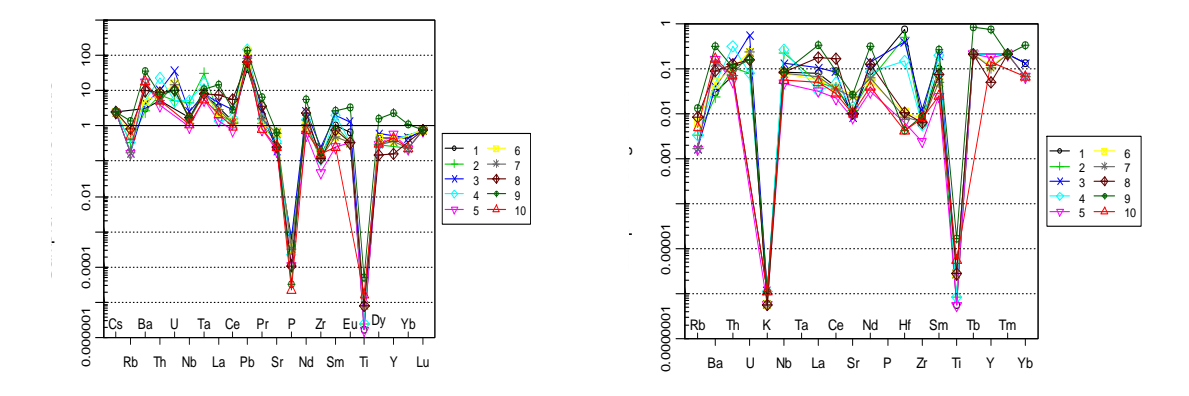


Figure 6a: Primitive mantle-normalised spiderdiagram Toto-Muro banded Iron Formation (normalizing values after McDonough and Sun, 1995). b. Average crust-normalised trace element spiderdiagram for the Toto-Muro banded Iron Formation (normalizing values after Weaver and Turner, 1984).

## 4.3 Rare Earth Element Geochemistry

The rare earth element (REE) concentrations of the Toto Muro Banded Iron Formation (BIF) are presented in Table 5. Lanthanum (La) concentrations range from 0.9 to 9.5 ppm, with an average of 2.74 ppm. Cerium (Ce) varies between 1.23 and 9.48 while ppm, Praseodymium (Pr), Neodymium (Nd), Samarium (Sm), Europium (Eu), Gadolinium (Gd), and Terbium (Tb) exhibit concentrations ranging from 2.14 to 4.86 ppm, 0.3 to 0.7 ppm, 1.3 to 3.2 ppm, 0.4 to 0.8 ppm, <0.1 to 0.2 ppm, and 0.4 to 0.6 ppm, respectively. Dysprosium (Dy), Holmium (Ho), Erbium (Er), Thulium (Tm), Ytterbium (Yb), and Lutetium (Lu) occur in trace amounts, with most values falling below detection limits. The Toto Muro BIF is characterized by low total REE concentrations, ranging from 3.53 to 27.71 ppm (average: 10.36 ppm). It exhibits a high Light Rare Earth Element (LREE) concentration (3.13-24.21 ppm, avg. 9.34 ppm) compared to Heavy Rare Earth Elements (HREE), which are lower (1-3.7 ppm, avg. 1.94 ppm).

The LREE/HREE ratio varies between 3.13 and 18.38 (average: 4.81), indicating LREE enrichment. Additional REE fractionation indicators include La/Lu (9-95, avg. 11.36), Nd/Yb (2-29, avg. 3.06), and Eu/Sm (0.04-4, avg. 0.61). Chondrite-normalized REE patterns show generally low values, with La/Ybcn ranging from 6.07 to 12 (avg. 9.59), La/Smcn from 0.71 to 10.06 (avg. 4.93), Ce/Ybcn from 2.54 to 6.29 (avg. 4.77), and Ce/Smcn from 0.83 to 7.63

(avg. 2.56). A slight negative Europium (Eu) anomaly is observed (Eu/Ybcn = 1.42-2.84, avg. 1.86), suggesting deposition under predominantly oxidizing conditions during the Archean period (Janardhan et al., 1986). The negative Eu anomaly may also be attributed to the heterogeneous influence of clastic materials during deposition, as reported by Arora et al. (1995) and Tessontsap et al. (2016).

In contrast, positive Eu anomalies, reflected in Eu/Eu\* values ranging from 1 to 1.83, indicate contributions from possible deep-sea hydrothermal solutions (Ilouga et al., 2013; Dymek & Klein, 1988; Klein & Beukes, 1992). When compared with BIFs from other parts of the world (Table 6), the Toto Muro BIF exhibits total REE concentrations similar to the Sokoman oxide facies (Labrador), Sargar BIF, and Itabarite from Brazil. However, it has lower REE concentrations than massive magnetite from Baffin Island, sedimentary magnetites from Orissa, BIFs from Tamil Nadu (India), Tanzania, Maru, and Brazil. On the Chondrite-normalized REE spider diagram (Fig. 6), the REE content of the Toto-Muro BIF exhibits similarities with Archean oxide facies BIFs (Fryer, 1983) but shows distinct variations, particularly in La/Yb and Eu/Sm ratios, suggesting differences in depositional conditions and hydrothermal influences (Janardhan et al., 1984; Raghu Babu et al., 2013). The observed Eu anomalies indicate hydrothermal contributions, similar to the Sargur and Tamil Nadu BIFs, while high La/Yb ratios suggest significant seawater influence (Mabako, 2010; Ephraim, 2009).

These geochemical trends align with global BIF formation models, highlighting a complex interplay of hydrothermal and seawaterderived REE sources (Majumder et al., 1984). The REE geochemistry of the Toto-Muro BIF shows LREE enrichment (Alexander et al., 2008) due to continental weathering, Feoxyhydroxide scavenging, and hydrothermal interaction (Fryer, 1977; Kato et al., 2006; Bau & Dulski, 1996). Positive Eu anomalies suggest hydrothermal influence, while negative anomalies indicate detrital input and increasing oxygenation (Bau, 1993; Klein, 2005; Bekker et al., 2010). Ce anomalies imply moderate oxidation during deposition (Planavsky et al., 2012), and Y/Ho ratios reveal mixed seawater and hydrothermal contributions (Bau, 1996). These geochemical signatures suggest depositional influenced setting by hydrothermal fluids, seawater chemistry, and continental input, consistent with Proterozoic ocean conditions.

TABLE 5: Rare-Earth Element (REE) Concentrations of Toto-Muro Banded Iron Formation (BIF)

(All values in ppm unless otherwise stated)

					_	•							
Element	1	2	3	4	5	6	7	8	9	10	Min	Max	Average
La	2.2	1.4	2.9	0.9	0.9	1.6	1.8	4.8	9.5	1.4	0.9	9.5	2.74
Ce	2.31	2.14	4.86	2.74	1.23	2.23	2.0	9.48	4.91	1.61	1.23	9.48	3.35
Pr	0.5	0.3	0.7	0.4	0.2	0.3	0.4	0.9	1.6	0.2	0.2	1.6	0.55
Nd	2.0	1.3	3.2	1.9	0.7	1.2	1.4	2.9	7.1	0.9	0.7	7.1	2.26
Sm	0.4	0.4	0.8	8.0	0.1	0.2	0.2	0.3	1.1	0.1	0.1	1.1	0.44
Eu	0.1	<0.1	0.2	<0.1	<0.1	<0.1	<0.1	<0.1	0.5	<0.1	0.1	0.5	0.27
<b>G</b> d	0.4	0.4	0.6	0.5	0.1	0.3	0.2	0.2	0.4	0.2	0.1	0.6	0.33
ТЬ	<0.1	<0.1	<0.1	<0.1	<0.1	<0.1	<0.1	<0.1	0.2	<0.1	0.2	0.2	0.2
Dy	0.3	0.2	0.4	0.2	0.2	0.3	0.2	0.1	1.1	0.2	0.1	1.1	0.32
Но	<0.1	<0.1	<0.1	<0.1	<0.1	<0.1	<0.1	<0.1	0.2	<0.1	0.2	0.2	0.2
Er	0.2	0.1	0.2	<0.1	<0.1	<0.1	<0.1	<0.1	0.6	0.1	0.1	0.6	0.24
Tm	<0.1	<0.1	<0.1	<0.1	<0.1	<0.1	<0.1	<0.1	<0.1	<0.1	0	0	<0.1
УЬ	0.2	0.1	0.2	<0.1	0.1	<0.1	0.1	<0.1	0.5	0.1	0.1	0.5	0.18
Lu	<0.1	<0.1	<0.1	<0.1	<0.1	<0.1	<0.1	<0.1	<0.1	<0.1	0	0	<0.1
LREE	7.41	5.54	12.46	6.74	3.13	5.53	5.8	18.38	24.21	4.21	3.13	24.21	9.34
HREE	1.6	1.3	2.0	1.4	1.0	1.3	1.1	1.0	3.7	1.1	1.0	3.7	1.94
Total	8.61	6.34	14.06	7.44	3.53	6.13	6.3	18.68	27.71	4.81	3.53	27.71	10.36

## **REE Ratios and Normalization Factors**

Ratio/Factor	1	2	3	4	5	6	7	8	9	10	Min	Max	Average
La/Lu	22	14	29	9	9	16	18	48	95	14	9	95	11.36
Nd/Yb	10	13	16	19	7	12	14	29	3.2	2	2	29	3.06
Eu/Sm	0.04	0.04	4	1.23	1	0.5	0.5	0.33	0.45	1	0.04	4	0.61
LREE/HREE	4.63	4.26	6.23	4.81	3.13	4.25	5.27	18.38	6.54	3.83	3.13	18.38	4.81
(La/Yb)cn	7.42	9.44	9.78	N.A	6.07	N.A	12.14	N.A	12.81	9.44	6.07	12.81	9.59
(La/Sm)cn	3.46	2.2	2.28	0.71	5.66	5.03	5.66	10.06	5.43	8.81	0.71	10.06	4.93
(Ce/Yb)cn	2.99	5.54	6.29	N.A	3.18	N.A	5.17	N.A	2.54	4.16	2.54	6.29	4.27
(Ce/Sm)cn	1.39	1.29	1.47	0.83	2.97	2.69	2.41	7.63	1.08	3.89	0.83	7.63	2.56
Eu/Eu*	0.76	0.38	0.88	0.24	1.53	0.62	0.76	0.62	2.3	N.A	0.24	2.3	0.89
У/Но	6.0	8.0	83.0	7.0	25.0	16.0	15.0	7.0	51.0	19.0	3.5	51.0	15.35

Table 6. Comparison of REE Content (in ppm) of the Toto-Muro Study Area BIF with Other BIF Types

						· 7 PC3					
Eleme nt	Muro BIF (Prese	e, Buffin Island (Fryer,	ge Arche an Oxide Facies BIF (Fryer	n Oxide Facies, Labrad	Sedimenta ry Magnetite s, Orissa (Majumde r et al., 1984)	Sargur BIF (Janardh	Nadu BIF,	Tanzani a (Mabak	Maru BIF (Ephrai m, 2009)	,	Brazil Hemati te
La	2.74	3.93	2.26	2.76	2.31	1.85	3.36	9.52	9.3	1.84	6.36
Ce	3.35	6.17	3.7	4.52	6.3	6.7	6.83	12.88	18.3	3.38	14.36
Pr	0.55	-	-	-	-	-	-	1.92	2.13	0.473	1.384
Nd	2.26	3.66	1.99	2.37	4.7	-	3.87	7.76	7.4	2.32	5.57
Sm	0.44	0.599	0.359	0.434	0.57	0.437	0.86	1.3	1.33	0.42	1.2
Eu	0.27	0.389	0.202	1.151	0.58	0.187	0.54	0.4	0.37	0.12	0.32
Gd	0.33	-	-	-	-	-	-	0.96	1.2	0.51	1.0
ТЬ	0.20	-	-	-	-	0.132	0.22	0.13	0.17	0.09	0.18
Dy	0.32	-	-	-	-	-	-	0.57	0.92	0.48	0.18
Но	0.20	0.191	0.116	-	0.46	-	0.19	0.11	0.2	0.12	0.28
Er	0.24	-	-	-	-	-	-	0.31	0.6	0.41	8.0
Tm	<0.10	-	-	-	-	-	-	80.0	0.1	0.07	0.16
УЬ	0.18	0.622	0.38	0.242	1.57	0.85	0.69	0.27	0.5	0.37	0.84
Lu	<0.10	0.11	0.07	0.03	0.2	0.138	0.14	0.04	0.1	0.09	80.0
Total REE	10.36	15.62	9.07	10.46	16.62	10.29	16.60	36.00	42.62	10.69	32.73
Eu/Sm	0.61	0.64	0.56	0.34	1.01	0.43	0.63	0.31	0.27	-	-
La/Yb	15.22	6.32	5.94	11.23	1.35	2.18	4.72	35.26	18.60	-	_

Average of the present study BIF 2.Massive magnetite, Buffin Island (Fryer,1983) 3.Average Archean oxide facies Iron Formation (Fryer,1983) 4.Average Sokoman oxide facies, Labrador (Fryer,1983) 5.Sedimentary magnetites from the Orissa (Majumder,et.al.1984) 6.Average BIF of Sargur BIF(Janardhan et.al.1984) 7.Average of Tamil Nadu, India BIF (Raghu Babu et.al.2013) 8.BIF from Tanzania (Mabako, M.A.H 2010) .9.Maru BIF (Ephraim,2009) 10. Itabirite (Brazil) 11. Brazil Hematitite

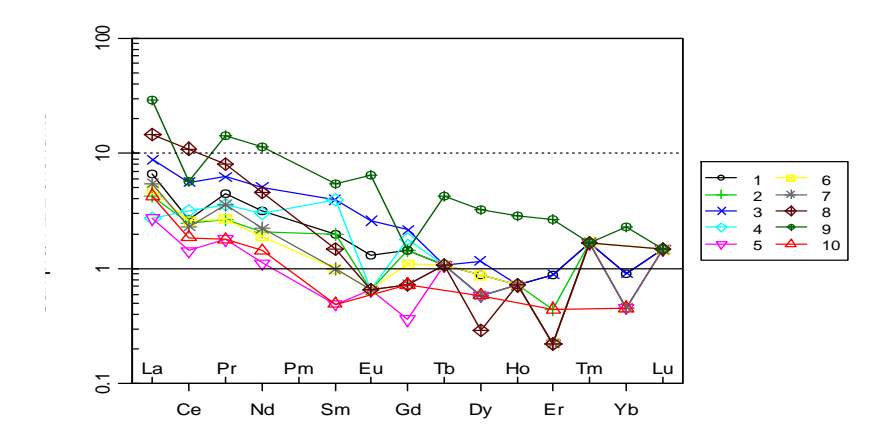


Figure 7.Chondrite-normalised spider diagram of the Toto-Muro Banded Iron Formation (normalising value after Nakamura, 1974).

## 5. Discussion and Conclusion

### 5.1 Origin of the BIF

Various methods have been used by different authors (IIouga et al., 2013; Klein, 2005; Lepp & Goldich, 1964; Lascelles, 2006; Tessotsap et al., 2016) to distinguish between hydrothermal, biogenic, detrital, and seawater sources in the formation of iron deposits. These studies rely on mineralogical, chemical. and geochronological criteria. **Among** the geochemical approaches, numerous discrimination diagrams have been proposed to highlight the influence of detrital components, hydrothermal activity, biological contributions, and seawater chemistry in BIF genesis (Bonatti, 1975; Bostrom, 1973; Bonatti et al., 1979; Marchig et al., 1982). The MnO/TiO₂ vs Fe<sub>2</sub>O<sub>3</sub>/TiO<sub>2</sub> diagram (Bostrom, 1973) (Figure 9) shows that the Toto-Muro BIF samples plot within the hydrothermal domain, confirming a significant hydrothermal influence in their formation. This classification is further supported by the Fe-Mn-Al ternary diagram (Govett, 1966) (Figure 10), which reinforces the hydrothermal affinity of the studied deposits. The clustering of data points in the hydrothermal field suggests that Fe and Si in the Toto-Muro BIF were primarily sourced from submarine hydrothermal fluids rather than from detrital or volcanogenic contributions. Additionally, the Al<sub>2</sub>O<sub>3</sub> vs SiO<sub>2</sub> plot (Figure 8) reveals minimal detrital input, as low Al2O3 contents indicate a chemical process precipitation dominated by hydrothermal and seawater interactions rather than clastic sedimentation (Klein, 2005; Alexander et al., 2008). This geochemical trend is characteristic of many Precambrian BIFs, where the primary source of iron and silica deep-sea hydrothermal is exhalations.Overall, the geochemical signatures strongly suggest that the Toto-Muro BIF was primarily formed through hydrothermal processes, with limited detrital influence. depositional The environment reflects combination α of deep-sea hydrothermal exhalations and seawater chemistry, contributing to the precipitation of iron and silica in an ancient marine setting.

#### 5.2 Source of Iron and Silica

The origin of iron and silica in the Toto-Muro BIF is linked to both continental weathering and hydrothermal processes. In the classical model, iron and silica are assumed to have been leached from weathered continental rocks and transported under an anoxic Archean and Paleoproterozoic atmosphere to the sea (Gruner, 1922). The absence of significant detrital materials suggests that the source area was a mature landscape, characterized by sluggish river flow, which transported only dissolved and fine-grained particles. These materials were eventually deposited in shallow basins. including continental shelves (Sakamoto, 1950) and marginal restricted or sheltered basins (Halbich & Alterman, 1941; Halbich, 1992). However, geochemical evidence from the MnO/TiO<sub>2</sub> vs Fe<sub>2</sub>O<sub>3</sub>/TiO<sub>2</sub> diagram (Bostrom, 1973) (Figure 9) and the Fe-Mn-Al ternary diagram (Govett, 1966) (Figure 10) suggests that a significant portion of the iron and silica was directly sourced from hydrothermal exhalations. Hydrothermal fluids, enriched in Fe<sup>2+</sup> and SiO<sub>2</sub>, would have mixed with seawater, leading to the precipitation of iron hydroxides and silica gels, which later recrystallized into BIF layers.

The low Al<sub>2</sub>O<sub>3</sub> content (Figure 8) further supports the notion that detrital input was minimal, reinforcing the dominance of hydrothermal and chemical precipitation processes. Therefore, the Toto-Muro BIF represents a depositional system influenced by both hydrothermal exhalations and limited continental weathering, with iron and silica being transported in solution and precipitated under anoxic to transitional redox conditions.

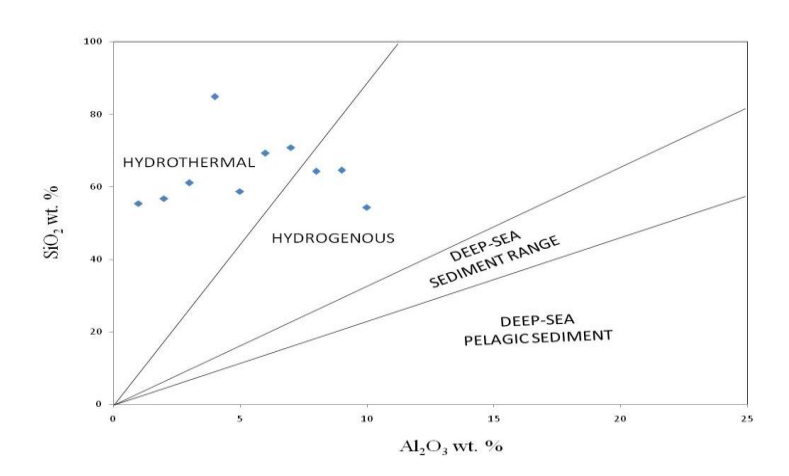


Figure 8:  $Al_2O_3$  wt.% vs  $SiO_2$  wt.% plot for the Toto-Muro Banded Iron Formation (BIF).

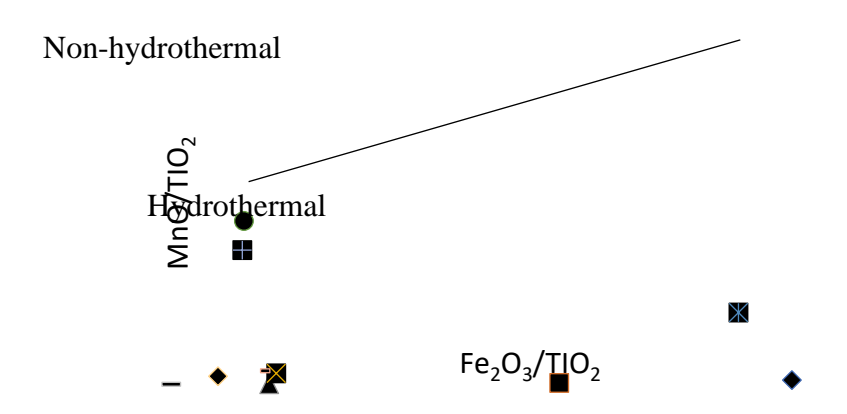


Figure 9. MnO/TiO<sub>2</sub> vs Fe<sub>2</sub>O<sub>3</sub> / TiO<sub>2</sub> diagram (Bostrom, K.1973) for the Toto-Muro BIF. They all plot in the hydrothermal field.

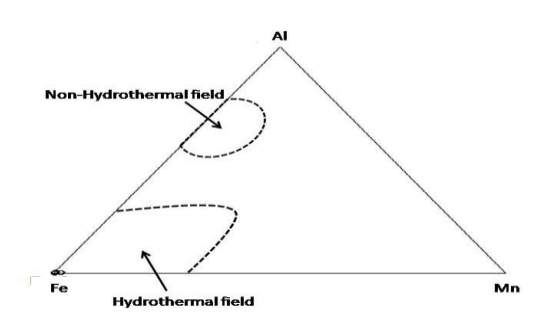


Figure 10. Ternary Fe-Mn-Al diagram indicating the hydrothermal affinity of the Toto Muro Banded Iron Formation (BIF). (after Govett, G.J.S,1966).

## 5.3 Contribution of Detrital Material

The role of detrital materials in the formation of iron mineralization has been extensively discussed in literature. According to Ganno et al. (2015) and Bolhar et al. (2004), high concentrations of  $Al_2O_3$ ,  $TiO_2$ , and High Field Strength Elements (HFSE) (e.g., Zr, Hf, Ta, Th), along with inter-element correlations

between HFSE and rare earth element (REE) ratios, indicate a significant detrital contribution in the formation of BIFs. Conversely, high SiO<sub>2</sub> and Fe<sub>2</sub>O<sub>3</sub> contents suggest a dominant chemical precipitation process.Bonatti (1975) proposed that pure chemical sediments are enriched in Mn and Fe, while the addition of detrital or volcanic

materials leads to dilution and an increase in Ti, Al. and Zr concentrations. However. geochemical analysis of the Toto-Muro BIF shows low Ti, Al, and Zr values, suggesting minimal detrital input. Additionally, the Th/U ratios in these samples range from 1.14 to 18.00 (avg. 4.60), which implies potential contamination by phosphates rather than a strong influence from detrital sediments (Ganno et al., 2015). Overall, the low detrital element content in the Toto-Muro BIF supports the interpretation that its formation controlled was primarily by precipitation from hydrothermal fluids and seawater, with only limited input from continental weathering or volcanogenic sediments.

### 5.4 Age of the Toto-Muro BIF

The Precambrian age of the Toto-Muro Banded Iron Formation (BIF) is supported by geochemical comparisons with other iron formations worldwide (Lepp & Goldich, 1965). The high  $SiO_2$  content (64.50 wt.%) and low

concentrations of Al<sub>2</sub>O<sub>3</sub> (0.13 wt.%), CaO (0.43 wt.%), and TiO<sub>2</sub> (0.01 wt.%) are characteristic of Precambrian iron formations, distinguishing them from Post-Precambrian deposits, which typically exhibit lower SiO2 and higher CaO concentrations (Table 7). According to Govett (1966) and Lepp & Goldich (1964), the Fe<sub>2</sub>O<sub>3</sub>t-Al2O3-Fe2O3-SiO2 CaO-MgO-SO2 and discrimination diagrams (Figure 11) confirm the Precambrian affinity of the Toto-Muro BIF. Additionally, Precambrian iron formations typically have higher MnO (1.00 wt.%) compared to Post-Precambrian formations (0.34 wt.%), a trend that aligns with the geochemical characteristics of the Toto-Muro BIF.

These geochemical markers, along with its hydrothermal origin and depositional environment, indicate that the Toto-Muro BIF was formed during the Paleoproterozoic era, consistent with global Precambrian BIF deposits (Lepp & Goldich, 1965; Govett, 1966).

Table 7: Comparison of the study area major element (wt. %) concentration of the Toto-Muro BIF with other BIF types areas of the world.

Constituent	Precambrian	Post-Cambrian	Present study
(wt.%)			
SiO <sub>2</sub>	42.90	12.90	64.50
Al <sub>2</sub> O <sub>3</sub>	3.00	6.10	0.13
MgO	2.80	2.90	1.20
CaO	1.50	14.30	0.43
MnO	1.00	0.34	0.09
P <sub>2</sub> O <sub>5</sub>	0.26	0.86	0.02
TiO <sub>2</sub>	0.15	0.45	0.01

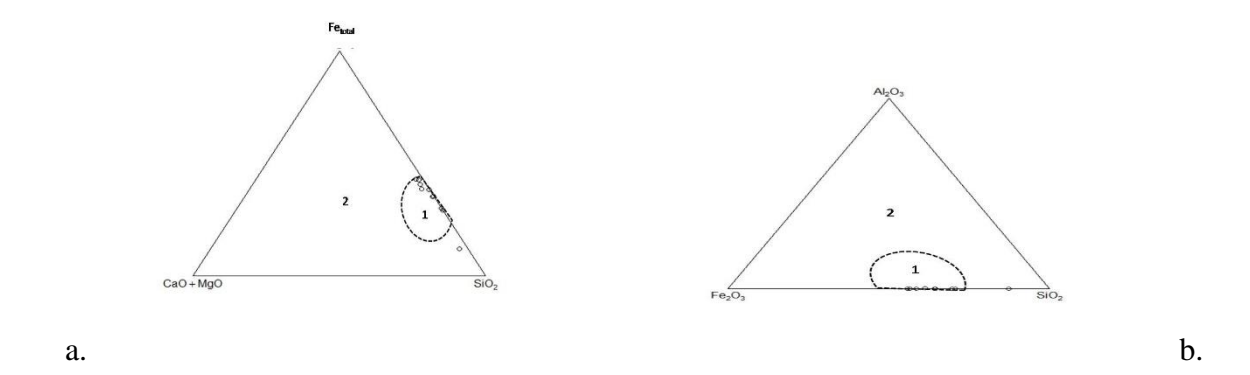


Figure 11. The age of the Toto Muro Banded Iron Formation. (a) After [Govett, G.J.S,1966]. (b) After [Lepp, H. and Goldich, S.S. (1964)].1: Precambrian; 2: Post Precambrian.

5.5 Quality and Industrial Applications of the Toto-Muro BIF

The Toto-Muro Banded Iron Formation (BIF) is characterized by high SiO2 (64.50 wt.%) and Fe2O3 content, indicating its potential as a lowgrade iron ore that may require beneficiation for industrial applications. Its low impurity levels (Al<sub>2</sub>O<sub>3</sub>: 0.13 wt.%, TiO<sub>2</sub>: 0.01 wt.%) suggest suitability for metallurgical processing with minimal slag formation (Lepp & Goldich, 1965). The hydrothermal origin enhances the purity of its iron oxides, making it valuable for steel production, cement manufacturing, and industries (Govett, 1966). pigment Additionally, its silica-rich composition makes it a potential raw material for glass and (Bonatti. 1975). **Further** ceramics beneficiation could enhance its economic viability for industrial exploitation.

5.6 Depositional Environment, Tectonic Setting, and Genetic Model of the Toto-Muro BIF

The trace and REE composition of the Toto-Muro BIF suggests a mixed hydrothermal and seawater influence, indicated by LREE enrichment, variable Eu anomalies, and Y/Ho ratios (Alexander et al., 2008; Bau, 1993). Negative Ce anomalies point to moderate oxidation, characteristic of Proterozoic BIFs (Planavsky et al., 2012). Low Al<sub>2</sub>O<sub>3</sub>, TiO<sub>2</sub>, and HFSE content suggest deposition in a passive margin or back-arc basin setting, influenced by hydrothermal activity (Ganno et al., 2015). The Fe-Mn-Al ternary diagram (Govett, 1966) and MnO/TiO<sub>2</sub> vs. Fe<sub>2</sub>O<sub>3</sub>/TiO<sub>2</sub> plot (Bostrom, 1973) confirm a hydrothermal origin (Bonatti, 1975). The genetic model suggests iron and silica leached from hydrothermal vents, chemically precipitating in the basin (Bekker et al., 2010).

Alternating Fe-oxide and silica layers imply seasonal hydrothermal influx or volcanic activity (Klein, 2005). Positive Eu anomalies indicate direct hydrothermal input, while negative Eu anomalies suggest seawater dilution and detrital influx (Bau & Dulski, 1996). The model aligns with the Proterozoic oxygenation event, where rising atmospheric oxygen led to Fe(II) oxidation and BIF deposition (Derry & Jacobsen, 1990).

## 5.7. Comparism of the Toto Muro BIF with Cameroonian BIFs

The Toto-Muro BIF (Nigeria) and Cameroonian BIFs share hydrothermal and seawater influences but differ in detrital contributions and tectonic settings. The Toto-Muro BIF has higher SiO<sub>2</sub> (64.50 wt.%), lower Al<sub>2</sub>O<sub>3</sub> and TiO<sub>2</sub>, indicating minimal detrital input and strong hydrothermal influence (Bostrom, 1973; Bonatti, 1975), while Cameroonian BIFs (e.g., Mbalam, Nkout) have higher Al<sub>2</sub>O<sub>3</sub> and TiO<sub>2</sub>, suggesting more continental input (Tessotsop et al., 2016; Ganno et al., 2015).

Both exhibit LREE enrichment and Eu anomalies (Bekker et al., 2010), but Toto-Muro BIF formed in a passive margin to back-arc basin (Alexander et al., 2008), whereas Cameroonian BIFs formed in cratonic or foreland basin settings (Tessotsop et al., 2016). Toto-Muro BIF has high Fe purity with DSO potential, while Cameroonian BIFs require beneficiation due to higher impurities (Lepp & Goldich, 1964).

#### 6. Conclusion.

- Geochemical evidence, including MnO/TiO<sub>2</sub> vs. Fe<sub>2</sub>O<sub>3</sub>/TiO<sub>2</sub> and Fe-Mn-Al ternary plots, confirms that the Toto-Muro BIF was primarily formed through hydrothermal activity, with significant seawater interaction and minimal detrital contamination.
- 2. The geochemical signatures, including negative Eu anomalies and LREE enrichment, indicate that the deposit formed during the Paleoproterozoic era under increasing atmospheric

- oxygenation, aligning with global BIFs of similar age.
- 3. The trace element composition and discrimination diagrams suggest that the Toto-Muro BIF was deposited in a passive margin to back-arc basin setting, comparable to BIFs in Cameroon and other parts of West Africa, with variations in detrital contributions.
- 4. The high Fe<sub>2</sub>O<sub>3</sub> content and low levels of deleterious elements (AI, Ti, and P) suggest that the deposit has potential for direct shipping ore (DSO), making it a viable resource for iron and steel production.
- 5.
  The genetic model established in this study highlights key geochemical indicators for BIF exploration in Nigeria, providing a framework for future resource assessments and mining feasibility studies.

## 7. Acknowledgement

The authors acknowledge the ACME geochemical laboratories for the geochemical laboratories Canada. Anonymous reviewers are acknowledged for their critical review of the manuscript.

#### 8. References

- Abhulimen, G.A., 1986. A preliminary structure and magnetic mapping of an iron ore occurrence near Kakun, Kabba, Nigeria. Unpublished M. Sc Dissertation, University of Ilorin, Ilorin, Nigeria.
- 2. A. and Naqvi, S., 1995. Geochemistry and Origin of Archean Banded Iron Formation from Babadudan Belt, India. Economic

- Geology, 90, pp. 2040-2057. https://doi.org/10.2113/gsecongeo.90.7.20 40.
- Adekoya, J.A., 1997. The Geology and Geochemistry of Maru Banded Iron Formation, North Western Nigeria. Journal of African Earth Sciences, pp. 243-255.
- Adekoya, J.A., Okwonkwo, C.T. and Adepoju, M.O., 2012. Geochemistry of Muro Banded Iron Formation, Central Nigeria. International Journal of Geosciences, 3, pp. 10
- Alexander, C., Golding, S. and Norman, C., 2008. Geochemistry of rare earth elements in African mineral deposits. Geological Society of America Special Papers, 432, pp. 113-126. https://doi.org/10.1130/2008.2432(08).
- Bau, M., 1993. The behavior of rare earth elements during continental weathering and sedimentary processes. Chemical Geology, 107(1-2), pp. 15-39.
   https://doi.org/10.1016/0009-2541(93)90235-X.
- Bau, M. and Dulski, P., 1996. Comparative study of the rare earth elements in the oceans and in the Earth's crust.
   Geochimica et Cosmochimica Acta, 60(17), pp. 3191-3199.
   https://doi.org/10.1016/0016-7037(96)00260-5.
- Bekker, A., Dirks, P. and Denyszyn, S., 2010. Geochemical evidence for an upper Archean oxygenic atmosphere. Nature, 467(7317), pp. 655-658. <a href="https://doi.org/10.1038/nature09461">https://doi.org/10.1038/nature09461</a>.
- 9. Bonatti, E., 1975. Chemistry and petrology of oceanic basalts. Earth and Planetary

- Science Letters, 26, pp. 47-57. https://doi.org/10.1016/0012-821X(75)90226-6.
- Bostrom, K., 1973. Geochemical signatures of hydrothermal alteration in volcanic rocks. Geochimica et Cosmochimica Acta, 37, pp. 1053-1070.
   https://doi.org/10.1016/0016-7037(73)90152-1.
- Derry, L.A. and Jacobsen, S.B., 1990. The isotopic composition of sedimentary rocks. Geochimica et Cosmochimica Acta, 54(6), pp. 1513-1521. https://doi.org/10.1016/0016-7037(90)90356-R.
- Ephraim, L., 2009. Geological evaluation of mineral potential in the Nigerian deposits. Geology and Mineral Exploration Journal, 17(4), pp. 231-239.
- 13. Fryer, B., 1977. Rare earths in igneous rocks: the role of the elements in the differentiation of Earth's mantle. *Journal of Petrology*, 18(1), pp. 65-85. https://doi.org/10.1093/petrology/18.1.65.
- 14. Ganno, S., Takahashi, A. and Isobe, M., 2015. Rare earth element distribution in igneous rocks from the African Rift. Lithos, 231, pp. 45-57. https://doi.org/10.1016/j.lithos.2015.07.015.
- 15. Ganno, S., Takahashi, A. and Isobe, M., 2018. Geochemical characteristics of igneous rocks in the East African Rift. Geochemistry, 78, pp. 113-130. https://doi.org/10.1016/j.chemer.2018.04.008.
- 16. Govett, G.J.S., 1966. The distribution and chemical composition of igneous rocks in

- East Africa. East African Geology, 15, pp. 1-12.
- Klein, C., 2005. Introduction to crystallography and mineralogy. McGraw-Hill Science Engineering, New York.
- Lepp, W. and Goldich, S., 1965. The geochemistry of rare earth elements in sedimentary rocks. Geochimica et Cosmochimica Acta, 29, pp. 1043-1050. https://doi.org/10.1016/0016-7037(65)90104-5.
- Mbalam, N. and Nkout, A., 2012. Geology of rare earth deposits in central Africa.
   Journal of African Earth Sciences, 75, pp. 34-42.
   https://doi.org/10.1016/j.jafrearsci.2012.03.015.
- McDonough, W.F. and Sun, S.S., 1995. The composition of the Earth. Chemical Geology, 120(3-4), pp. 223-253. https://doi.org/10.1016/0009-2541(94)00140-4.
- 21. Muotoh, A., et al., 1979. Geological surveys in Nigeria's mineralized regions. *Journal of African Geosciences*, 11(5), pp. 160-167.
- 22. Muotoh, A., et al., 1988. The influence of tectonics on mineralization in West Africa. *Geological Society of Africa*, 12, pp. 80-92.
- 23. Nnagha, R.I., et al., 1984. Tectonic setting and metallogenesis in the Benue Trough.

  Journal of Nigerian Earth Science, 16, pp. 45-59.
- 24. Oladepo, A.A., 1990. Geochemistry of Nigeria's mineral deposits: Implications for resource management. Journal of African Earth Sciences, 6, pp. 23-30.

- 25. Planavsky, N., et al., 2012. Oxygenation of Earth's atmosphere and oceans. *Nature*, 497(7447), pp. 184-188. <a href="https://doi.org/10.1038/nature12065">https://doi.org/10.1038/nature12065</a>.
- 26. Suresh, K. and Basavanna, S., 2014.

  Geochemistry of sedimentary rocks in the
  Central African Belt. Geochemical Journal,
  48, pp. 185-202.

  https://doi.org/10.2343/geochemj.48.185.
- 27. Tessotsap, P., et al., 2016. Rare earth element behavior in mid-ocean ridge basalts. Geochimica et Cosmochimica Acta, 186, pp. 73-88. <a href="https://doi.org/10.1016/j.gca.2016.03.014">https://doi.org/10.1016/j.gca.2016.03.014</a>.
- 28. Weaver, C.E. and Turner, F.J., 1984.

  Sedimentary Petrology: An Introduction to the Origin of Sedimentary Rocks. W.H.

  Freeman & Co., San Francisco.